Nanoscale Advances

ROYAL SOCIETY OF CHEMISTRY

PAPER

View Article Online
View Journal | View Issue

Cite this: *Nanoscale Adv.*, 2022, **4**, 2029

Zn-assisted modification of the chemical structure of N-doped carbon dots and their enhanced quantum yield and photostability†

Sohee Yun, Eun Soo Kang and Jin-sil Choi *

This article presents the Zn-assisted synthesis of N-doped carbon dots (**N-CDs**) with an enhanced quantum yield (QY) and photostability. There have been intensive studies to improve or tune the optical properties of carbon dots (CDs) to meet the demand for luminescent materials in various fields, including energy conversion, photocatalysis, bioimaging, and phototherapy. For these applications, the photostability of the CDs is also a critical factor, but the related studies are relatively less common. The Zn-assisted **N-CDs** (denoted as **Zn:N-CDs**) obtained by the addition of $Zn(OAc)_2$ to the precursors during the synthesis of **N-CDs** not only exhibited an enhanced quantum yield but also improved photostability compared to those of **N-CDs**. A comprehensive study of the chemical composition of **Zn:N-CD** and **N-CD** using X-ray photoelectron spectroscopy indicated a correlation between their chemical structure and photostability. $Zn(OAc)_2$, which acts as a catalytic reagent, induced the modification of chemical structures at the edges of carbogenic sp^2 domains, without being doped in **N-CD**, and the heteroatom–carbon bonds in **Zn:N-CD** seemed to be more resistant to light compared to those in **N-CDs**. The increased QY and photostability of **Zn:N-CDs** make them more suitable as an optical probe and they could be used in fingerprint identification. With **Zn:N-CDs**, the microstructure of fingerprints was confirmed clearly for a long duration effectively.

Received 7th January 2022
Accepted 9th March 2022

DOI: 10.1039/d2na00013j

rsc.li/nanoscale-advances

Introduction

Carbon dots (CDs) are considered promising nanomaterial candidates in various fields, including energy, optics, biology, and medicine, owing to their unique properties, low toxicity, ease of preparation, and cheap and abundantly available precursors.[1–3] The physicochemical properties of CDs are closely related to their atomic composition, chemical structure, and size, and extensive efforts have been made to improve their properties. In particular, the optical properties of CDs can be controlled by modulating the size of the carbogenic sp^2 domains, the shape of the domain edges, surface functional groups, or the type of metal dopant or fluorescent dye incorporated in the structure.[4–6] Owing to the quantum confinement effect, the band gaps of CDs are determined by the number of aromatic rings in their structure (*i.e.*, the size of the carbogenic domains in the CD).[7,8] The surface passivation of CDs by doping heteroatoms such as B, N, or S can increase their fluorescence quantum yield (QY) from ~2 to as high as 70–90%.[9–13] The doping of metals such as Zn, Ni, and Mn can also increase the QY of CDs.[14,15] Furthermore, the deoxidation of CDs using UV light can reduce the nonradiative recombination of excitons at the surface and thus enhance their QY.[16] The types of functional groups at the edges of the sp^2 domains play a critical role in determining the optical properties of CDs.[17–19] In addition, the distribution of –COOH or $–NH_2$ groups at the sp^2-domain edges of CDs is known to change the energy level of the frontier orbitals, causing a change in the emission wavelength.[20] Consequently, CDs with enhanced QYs and adjustable maximum emission wavelengths are broadly applied in various areas, including energy conversion, photocatalysis, bioimaging, and phototherapy.

Photostability is another critical issue to be considered when developing CDs for certain applications. CDs are known to have better photostability than molecular optical probes, but they become unstable under long-term exposure to light.[21–23] Continuous UV excitation leads to changes in the chemical structures within CDs, resulting in a decrease in the QY.[24] In addition, it has been reported that the photodegradation of CDs can cause cytotoxicity.[25] To resolve these issues, various studies have attempted. According to one study, polymer membranes can prevent the photodegradation of CDs under continuous exposure to light.[26,27] Another study showed that the addition of ascorbic acid, which acts as a reducing agent and radical

Department of Chemical and Biological Engineering, Hanbat National University, Daejeon 34158, Korea. E-mail: jinsil.choi@hanbat.ac.kr

† Electronic supplementary information (ESI) available: TEM images of **N-CDs**, excitation-dependent emission of **Zn:N-CDs**, QY measurements of Zn–N-CDs and **N-CDs**, analysis of the content of Zn ions in **Zn:N-CDs** using ICP-MS, IR spectra of **N-CDs** and **Zn:N-CDs**, relative atomic compositions of **Zn:N-CDs** and **N-CDs** determined using XPS, and zeta potential and toxicity assay of **Zn:N-CDs**. See DOI: 10.1039/d2na00013j

scavenger, can also retard the fluorescence bleaching rate of CDs.[28] Furthermore, CDs prepared at high reaction temperatures and/or for long reaction times have been demonstrated to exhibit lower photobleaching rates upon exposure to light than CDs synthesized under milder conditions.[29,30] Although these studies achieved progress to improve the photostability of CDs, they were conducted recently, and further studies are required to develop photostable CDs.[23] Furthermore, in many studies on the photostability of organic materials, it has been identified that the chemical structure is one of the critical factors that determine their photostability.[31–33] However, the relationship between the chemical structure of CDs and their photostability is not fully understood yet.

In this study, we prepared N-doped CDs (**N-CD**s) by adding $Zn(OAc)_2$ to the CD precursors in the synthetic step. The Zn-assisted **N-CD**s (denoted as **Zn:N-CD**s) exhibited significantly enhanced QY and photostability compared to those of **N-CDs** synthesized without using the Zn salt. Many studies have demonstrated that the doping of the Zn(II) ion in CDs can improve their optical properties.[14,24,34–37] However, in this study, $Zn(OAc)_2$ was not incorporated in the **Zn:N-CD** matrix, as ascertained through inductively coupled plasma-mass spectrometry (ICP-MS) analysis. Instead, it changed the chemical structure of certain domains in the **Zn:N-CD**s compared to those of **N-CD**s, leading to enhanced QY. Additionally, the study of the chemical structure before and after light exposure clearly indicated that the difference in the photostabilities of **Zn:N-CD**s and **N-CD**s is closely related to the structural differences between them. Thus, the developed **Zn:N-CD**s could be used to successfully visualize the detailed structure of a latent fingerprint over a five times longer duration than that provided by **N-CD**s.

Experimental section

Reagents

Citric acid (CA, 99.9%), ethylenediamine (EDA, >98%), zinc acetate [$Zn(OAc)_2$, 98.0%], quinine sulfate (98.0%), and the 3-(4,5-dimethylthiazol-2-yl)-2,5-diphenyltetrazolium bromide (MTT) assay kit were purchased from Sigma Aldrich and used as received. A549 cells were purchased from American Type Culture Collection (USA) and grown in Dulbecco's modified eagle medium supplemented with 10% fetal bovine serum.

Synthesis of N-CD and Zn:N-CDs

N-CDs and **Zn:N-CD**s were prepared according to a previously reported method with some modifications.[38,39] In a typical synthesis, CA (10 μmol) and EDA (5 μmol) were dissolved in deionized water (15 mL) for both **N-CD** and **Zn:N-CD**s. $Zn(OAc)_2$ (0.1–5 μmol) is further added for **Zn:N-CD**s, and the resulting mixture was hydrothermally treated in a Teflon-lined stainless steel autoclave at 200 °C. After one hour of the reaction, the mixture was cooled to room temperature, and the residue was purified by column chromatography (CombiFlash NextGen 100, Teledyne ISCO) to obtain a brown **Zn:N-CD** sample.

Material characterization

The size and morphology of **Zn:N-CD** were examined by transmission electron microscopy (TEM, Hitachi, H-7650). The Zn content and crystalline structure of **Zn:N-CD** were analyzed by ICP-MS (NEXION-350X, PerkinElmer Korea) and X-ray diffraction (XRD, SmartLab, Rigaku, Japan), respectively. The chemical functional groups and composition of **Zn:N-CD**s were investigated by Fourier-transform infrared (FTIR) spectrometry (Nicolet 6700, Thermo, USA) and X-ray photoelectron spectroscopy (XPS, K-Alpha+, Thermo Fisher Scientific, USA), respectively. The absorption and fluorescence spectra of **Zn:N-CD**s were recorded using a UV-vis spectrophotometer (Lambda 1050, PerkinElmer) and fluorescence spectrometer (QM-400, HORIBA), respectively. The fluorescence lifetime was measured using a fluorescence lifetime spectrometer (FL920, Edinburgh Instruments, United Kingdom).

QY measurements

The relative QYs of **Zn:N-CD**s and **N-CD**s were calculated as follows:

$$Q_s = Q_r \frac{m_s}{m_r} \frac{n_s}{n_r}$$

where Q is the fluorescence QY, m is the slope of the plot of the integrated fluorescence intensity against absorbance, and n is the refractive index of the solvent. The subscripts s and r represent the sample and reference, respectively. A solution of quinine sulfate in a 0.5 M H_2SO_4 aqueous solution was used as the reference (QY = 54.6%). The QY was determined through an average of three measurements under consistent experimental conditions.

In vitro cell viability assay

The biocompatibility of the **Zn:N-CD** and **N-CD** samples was evaluated using human lung cancer cells (A549) using the MTT assay. A549 cells (2×10^5 cells per well) were cultured overnight in a 96-well microtiter plate in a 5% CO_2 atmosphere at 37 °C. The wells were charged with a cell medium containing **Zn:N-CD** or **N-CD** (12.5, 25.0, 50.0, 75.0, 100.0, 250.0, and 500.0 μg mL^{-1}) and incubated for 24 h. Then, 10 μL of the MTT solution was added to each well (final concentration: 0.5 mg mL^{-1}). After incubation for 4 h, formazan, which is generated from the reduction of MTT with NAD(P)H-dependent oxidoreductase in living cells, was dissolved in the solubilization solution provided with the kit. The absorbance at 550 nm was obtained using a microplate reader (SpectraMax M2e, Molecular Devices, LLC, USA).

Fingerprint analysis using the CDs

A drop of the aqueous solution containing **Zn:N-CD** or **N-CD** (0.5 mg mL^{-1}) was cast on fingerprints on a glass slide. Subsequently, the solvent was evaporated, and the fingerprints were observed using a UV lamp (365 nm, 400 μW cm^{-2}).

Results and discussion

Zn:N-CD was prepared as reported previously with some modifications.[38,39] $Zn(OAc)_2$ was added to the reaction solution containing CA and EDA (Fig. 1a). The synthesized **Zn:N-CD** was confirmed to have a spherical shape and an average size of 3.5 ± 1.1 nm, as shown in the TEM image (Fig. 1b). The size of **Zn:N-CD** was found to be slightly smaller than that of **N-CD** (5.9 ± 1.3 nm) (Fig. S1, ESI†). High-resolution TEM images revealed that **Zn:N-CD** has a partially crystalline structure with a lattice spacing of 0.2 nm, which corresponds to the spacing of the (100) plane of graphite (Fig. 1c).[40,41] In Fig. 1d and S2,† the XRD patterns of **Zn:N-CD** and **N-CD** exhibit a broad diffraction peak centered at ~19.58°, which is attributed to the (002) lattice spacing of a typical carbon-based material (JCPDS # 26-1076).[42–44]

The optical properties of **Zn:N-CDs** were explored by analyzing their absorption and emission spectra. Both the **Zn:N-CD** and **N-CD** samples yielded absorption peaks at 240 and 340 nm, corresponding to the π → π* transition of the sp^2 domains (–C=C–) and n → π* transition of the C=O groups at the edge of sp^2 domains, respectively (Fig. 2a).[1,3,40] **Zn:N-CD** showed a clearer shoulder peak at 240 nm compared to that of **N-CD**. The fluorescence spectra (λ_{ex}: 350 nm, Fig. 2b) of **N-CD** and **Zn:N-CD** exhibited strong emission peaks at 445 and 450 nm, respectively. The emission spectrum of **Zn:N-CD** was broader than that of **N-CD**, implying that the optical transitions in **Zn:N-CD** involved a wider distribution of electronic states compared to those in **N-CDs**.[45] A continuous red shift in the emission maximum of **Zn:N-CD** was observed with the increase in the excitation wavelength (Fig. S3, ESI†). This excitation-dependent emission of **Zn:N-CDs** arises from surface energy trap states, which turn emissive upon surface passivation.[45–47]

When placed on a UV lamp (λ_{ex}: 365 nm, UVItech, England), both the **Zn:N-CD** and **N-CD** samples displayed a bright blue color. Several **Zn:N-CD** samples were synthesized using different amounts of $Zn(OAc)_2$ at a fixed CA : EDA ratio (2 : 1). As shown in Fig. 3a and S4,† the brightness of the aqueous suspension of **Zn:N-CDs** varied depending on the amount of $Zn(OAc)_2$ used in the synthesis. The emission spectra of the suspensions in the same concentration clearly exhibited a brightness variation (Fig. S5, ESI†). The relative QYs (standard: quinine sulfate in a 0.5 M H_2SO_4 aqueous solution) of the **Zn:N-CD** samples were measured to be 31.6%, 34.4%, 41.5%, 47.4%, 36.4%, 36.4%, and 31.9%, respectively, when the ratio of EDA : $Zn(OAc)_2$ was increased from 1 : 0 to 0.02, 0.04, 0.125, 0.25, 0.5, and 1 (Fig. 3b). **Zn:N-CDs** synthesized with an EDA : $Zn(OAc)_2$ ratio of 1 : 0.125 exhibited the highest QY among the **Zn:N-CD** samples, and the value was approximately 1.5 times higher than that of **N-CD** (31.6%). **Zn:N-CD** showed a slightly slower fluorescence decay rate (1.13 ns) than **N-CD** (0.84 ns) under 350 nm excitation (Fig. 3c). It has been reported that the extended fluorescence lifetime of CDs, which results from a decrease in the nonradiative recombination and self-trapping of excitons, contributes to QY enhancement.[46,48–50] The QYs of **N-CD** samples synthesized using other Zn sources, *viz.*, $ZnSO_4$, $ZnCO_3$, $ZnCl_2$, $Zn(NO_3)_2$, and $Zn(BF_4)_2$, were determined to be 27, 35, 25, 21, and 38%, respectively (Fig. S6, ESI†). The addition of acetic acid, NaOAc, or other metal sources (*i.e.*, $Mn(OAc)_2$, $Fe(OAc)_2$, and $Cu(OAc)_2$) did not result in improved QY of the obtained **N-CDs** (Fig. S6, ESI†). In addition, **N-CDs** prepared without the assistance of the Zn salt in the synthetic step retained their QY (35%) after post-reaction with $Zn(OAc)_2$

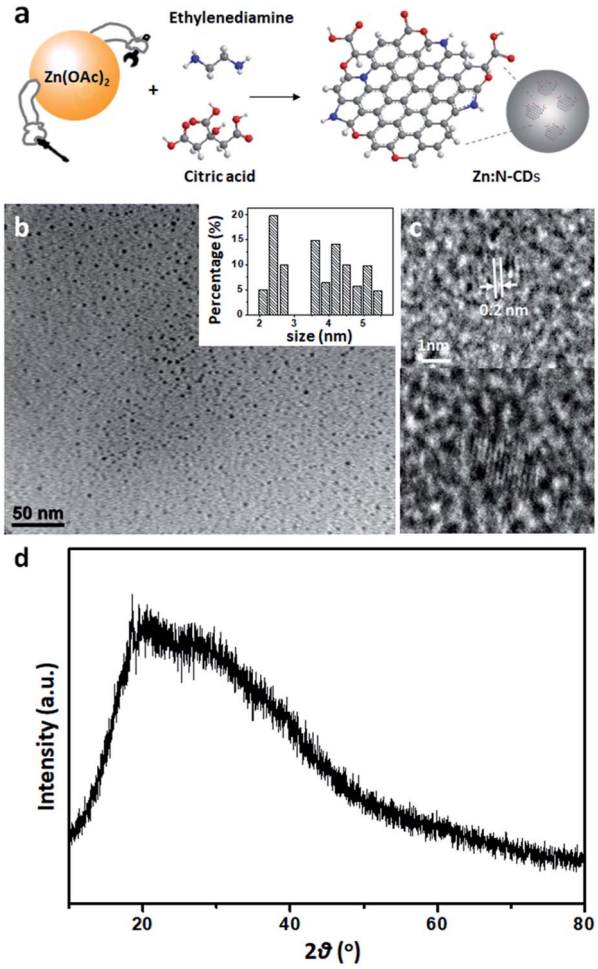

Fig. 1 (a) Schematic of **Zn:N-CD** synthesis. Each sphere represents an atom as follow: white: H, grey: C, blue: N, and red: O. (b) Low-resolution and (c) high-resolution transmission electron microscopy images of **Zn:N-CD**. Inset in (b) shows the particle size distribution. (d) XRD pattern of **Zn:N-CD**.

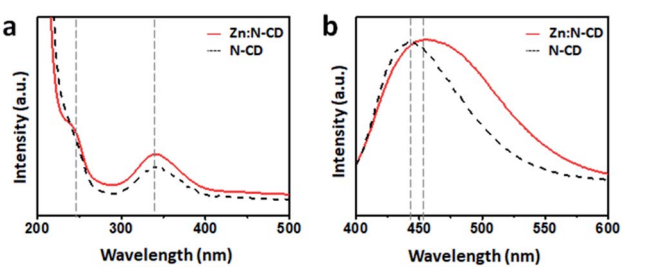

Fig. 2 (a) Normalized absorption and (b) emission spectra of the **Zn:N-CD** and **N-CD** samples.

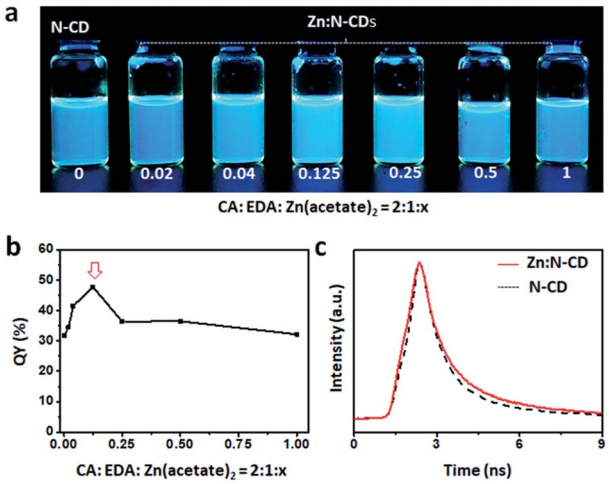

Fig. 3 (a) Photograph of the suspensions of Zn:N-CDs and N-CD (conc.: 0.5 mg mL^{-1}) placed on top of a UV lamp (365 nm). (b) Quantum yields and (c) fluorescence lifetimes of Zn:N-CDs and N-CD (λ_{ex} = 350 nm and λ_{em} = 450 nm).

(Fig. S6, ESI†). Therefore, $Zn(OAc)_2$ seems to play an important role in the synthetic stage of **Zn:N-CD** to improve their optical properties.

The photostability of **Zn:N-CD** was examined with light exposure. Aqueous suspensions containing **Zn:N-CD** or **N-CD** (0.1 mg mL^{-1}) were exposed to daylight for 48 h, and their fluorescence intensity at 450 nm (λ_{ex}: 350 nm) was measured using a fluorometer. As shown in Fig. 4a, the **Zn:N-CD** suspension retained ~80% of its initial fluorescence intensity after 8 h of exposure, while the fluorescence intensity of the **N-CD** suspension decreased to ~40%. Overall, the fluorescence intensity of the **Zn:N-CD** suspension decreased slowly under daylight compared to that of the **N-CD** suspension. **Zn:N-CD** also exhibits higher photostability compared to various **N-CDs**

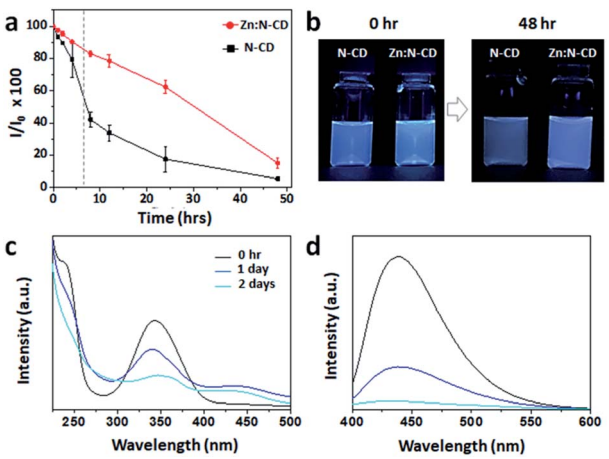

Fig. 4 (a) Time-dependent fluorescence intensities of Zn:N-CD and N-CD under exposure to daylight (λ_{ex}: 350 nm and λ_{em}: 450 nm). (b) Images of the aqueous suspensions of Zn:N-CD and N-CD before and after exposure to daylight. (c and d) Absorption and emission spectra of Zn:N-CD before and after exposure to daylight.

(Fig. S7, ESI†). Although the fluorescent intensity of the **Zn:N-CD** and **N-CD** samples decreased to 13 and 5% of their initial fluorescence intensity, respectively, after 48 h of exposure to daylight, **Zn:N-CD** exhibited relatively high fluorescence owing to its superior initial intensity, as shown in Fig. 4b and S5.† Therefore, we inferred that $Zn(OAc)_2$ plays a vital role in the formation of the **Zn:N-CD** structure to improve its photostability compared to that of **N-CD**. In the absorption spectrum of **Zn:N-CD**, the intensities of the peaks at 250 and 340 nm decreased significantly with light exposure (Fig. 4c). Meanwhile, the absorption of **Zn:N-CD** at ~275 and 450 nm increased after one day of light exposure. In the fluorescence spectrum, the fluorescence intensity at 450 nm decreased with light exposure, without any peak shift (Fig. 4d).

To understand the role of $Zn(OAc)_2$ in the formation of **Zn:N-CD**, the chemical structures of the **Zn:N-CD** and **N-CD** samples were investigated through FTIR spectroscopy and XPS. $Zn(OAc)_2$ appeared to only participate in the formation of **Zn:N-CD**, without being incorporated in the CD framework, as inferred from the negligible Zn content in the ICP-MS analysis (Table S1, ESI†). The FTIR spectra revealed that **Zn:N-CD** and **N-CD** consist of similar functional groups (Fig. S8, ESI†). However, the peak at 895 cm^{-1} corresponding to the C–O–C groups in the glycosidic structure,[51,52] which was observed in the spectrum of **N-CD**, did not appear in the FTIR spectrum of **Zn:N-CD**. In addition, a new peak at 1038 cm^{-1}, originating from C–O bonding in polysaccharides,[53] appeared newly in the FTIR spectrum of **Zn:N-CD**. In addition, **Zn:N-CD** possessed less negative surface charge compared to **N-CD**, indicating fewer carboxylic groups on its surface (Table S2, ESI†). The chemical compositions of the **Zn:N-CD** and **N-CD** samples were further analyzed using XPS. In the survey XPS scan of **Zn:N-CD**, peaks from C_{1s}, N_{1s}, and O_{1s} were observed clearly, and no peak of Zn_{2p} was present, which is consistent with the result of the ICP-MS analysis. Based on the area of each peak in the XPS spectra (Fig. 5 and S9, ESI†), it was determined that **Zn:N-CD** has a slightly higher C_{1s} content (63.1%) than **N-CD** (59.3%), while the contents of the other atoms in **Zn:N-CD** were slightly lower than those in **N-CD** (N_{1s}: 7.5% and O_{1s}: 29.4% in **Zn:N-CD** *vs.* N_{1s}: 8.7% and O_{1s}: 32.0% in **N-CD**). The chemical bonding of each atomic component was investigated in detail through a spectral peak fitting of the high-resolution C_{1s}, N_{1s}, and O_{1s} spectra based on the reported binding energies of the chemical bonds, as shown in Fig. 5. In the C_{1s} spectrum of **Zn:N-CD** (Fig. 5a), a strong peak is observed at 284 eV, corresponding to the C–C/C=C bonds of the carbogenic domains, along with the peaks of C–O (285.5 eV) and C=O (288.0 eV). In the N_{1s} spectrum (Fig. 5a), **Zn:N-CD** shows a strong peak for $N_{pyrrole}$ (399.5 eV) located at the edge sites of the carbogenic domain and a negligible peak (401 eV) for $N_{graphite}$ located in the sp^2-carbon domain. Furthermore, the O_{1s} spectrum contains two peaks corresponding to the C–O and C=O bonds (532.6 and 531.1 eV, respectively) (Fig. 5a). The results indicate that **Zn:N-CD** contains a higher population of carbons in the carbogenic domains and a negligible amount of graphitic N compared to **N-CD** (Fig. 5a and b). The coordination of the carbon precursors (CA and EDA) around Zn ions might

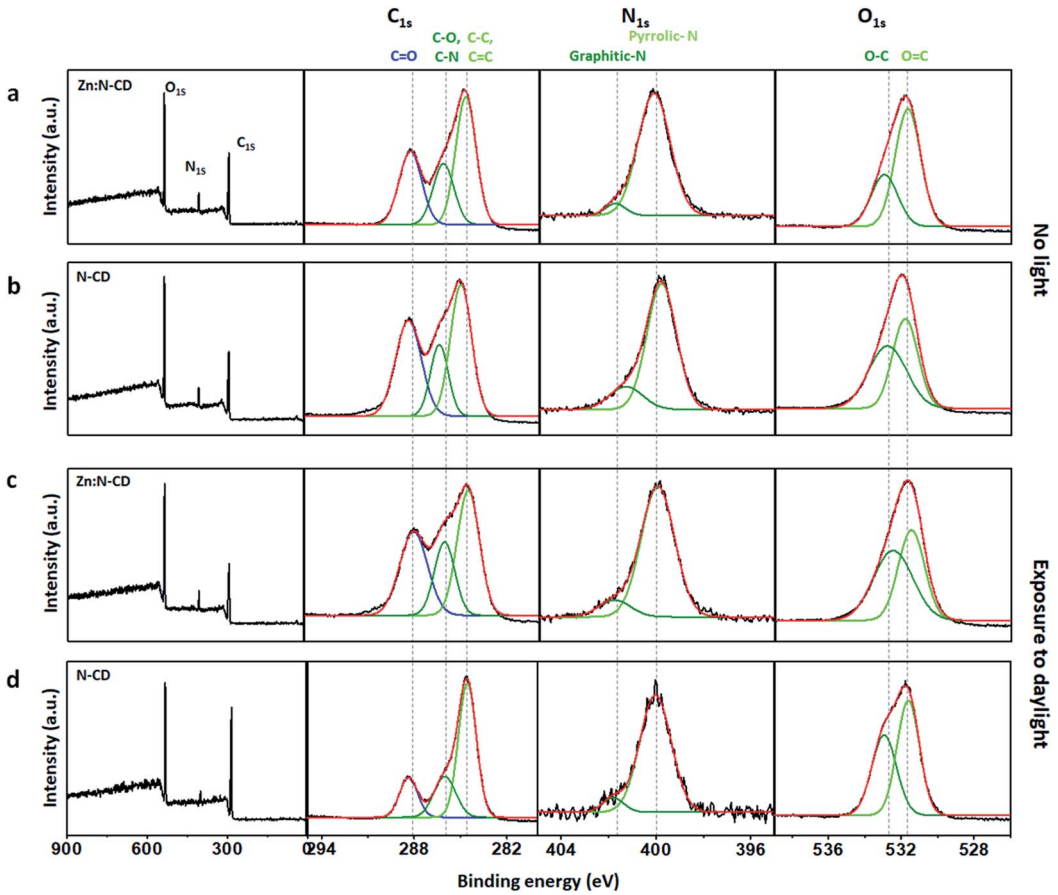

Fig. 5 XPS survey scans and high-resolution C_{1s}, N_{1s}, and O_{1s} spectra of **Zn:N-CDs** (a and c) and **N-CDs** (b and d) before light exposure (a and b) and after exposure to daylight (c and d).

have aided the formation of carbogenic domains in **Zn:N-CD**.[37,54]

Interestingly, after exposure to light, the chemical compositions of **Zn:N-CD** and **N-CD** differed substantially, as shown in Fig. 5c and d. **Zn:N-CD** had a similar atomic composition before and after 48 h of exposure to daylight (Fig. S9, ESI†). According to the detailed analysis of the chemical bonding of **Zn:N-CD**, its overall chemical composition before and after light exposure was almost similar, although the peak intensity from C–C/C=C and C=O bonding decreased slightly. These structural changes induce the absorbance variation (Fig. 4c) originating from new energy states.[5,17,55] The photodegradation of **Zn:N-CD** seems to induce impurities in the cariogenic domains, leading to an absorption intensity increase at ~275 nm.[17] The increase of the C–O ratio in **Zn:N-CD** induced the absorption peak decrease at 350 nm (n → π* transition of C=O) (Fig. 5c) and the rise of newly appeared absorbance at approximately 450 nm.[5,55] Conversely, the atomic content of C in **N-CD** increased significantly from 59% to 72% after exposure to light, whereas those of N and O decreased (N_{1s}: 32% to 25% and O_{1s}: 9% to 3%; Fig. S9, ESI†). In the C_{1s} spectrum of **N-CD** after light exposure (Fig. 5d), peaks from carbon and heteroatom bonding were considerably decreased in strength. Possibly, reduced surface passivation of the carbogenic domains in **N-CD** resulted in a decrease in the emission.[1,6,48,49] These results indicated that the photostability of the carbon and heteroatom bonds in **Zn:N-CD** and **N-CD** differed significantly under light exposure. $Zn(OAc)_2$ is known to be a Lewis acid that can act as a catalyst in esterification, amide oxidation, and hydroacylation reactions.[56,57] Therefore, it can be inferred that, in the synthetic step, $Zn(OAc)_2$ participated in the reaction between the precursors, leading to chemical modification of the edge functional groups in **Zn:N-CD**. As a result, the photostability of **Zn:N-CD** was significantly enhanced compared to that of **N-CD**.

Zn:N-CDs with enhanced QY and photostability can be used as optical tags in various applications. One of their potential applications is in the identification of latent fingerprints.[2,10,58,59] **Zn:N-CD**s can successfully adsorb to fingerprints through the interaction of their hydrophobic sp^2 domains with the oil component contained in the fingerprint.[2,58,59] In addition, negatively charged **Zn:N-CD**s effectively interact with basic proteins of the secretion components (Table S2, ESI†).[58] When the aqueous suspension of **Zn:N-CD** (0.5 mg mL^{-1}) was deposited and dried on the substrate with the fingerprints, **Zn:N-CD** could successfully increase the contrast of the latent fingerprints (Fig. 6a). **Zn:N-CD** provided a clear view of the detailed structures of the fingerprints, such as the core, fork, and ending ridge features, as shown in the magnified images of Fig. 6a(ii)–

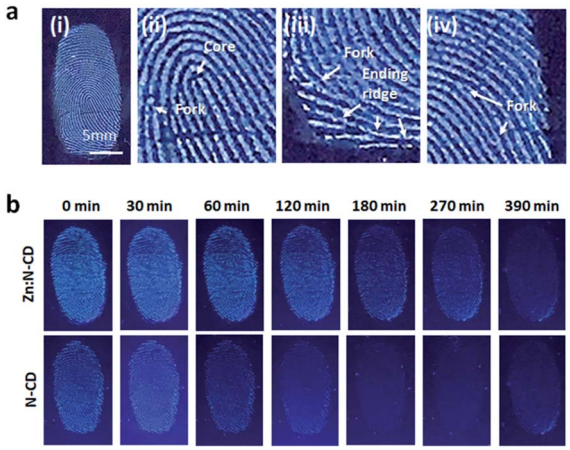

Fig. 6 (a) Latent fingerprint images visualized using **Zn:N-CDs**. (b) Images of the fingerprints visualized using **Zn:N-CDs** and **N-CDs** at different time points.

(iv). In addition, when the same amounts of the **Zn:N-CD** and **N-CD** aqueous suspensions were used, the fingerprint adsorbed with **Zn:N-CD** yielded a brighter signal than that adsorbed with **N-CD** owing to the higher QY of the former. Furthermore, the detailed structure of the fingerprint stained with **Zn:N-CD** could be confirmed for up to 6.5 h, while it was hardly distinguishable after 2 h when stained with **N-CD** (Fig. 6b). Although continuous UV light irradiation reduced the fluorescent signal from **Zn:N-CD** and **N-CD** faster compared to daylight, **Zn:N-CD** can still visualize fingerprints efficiently for a longer period of time compared to **N-CD** (Fig. S10 and S11, ESI†). In fingerprint identification, it is essential to minimize background signal interference,[2,58,59] so that the strong fluorescent signal of **Zn:N-CD** can effectively differentiate the microstructure of the fingerprints from various background signals for accurate fingerprint identification. In addition, the stable emission of **Zn:N-CD** under various light conditions enables fingerprint identification for an extended period of time compared to **N-CD**. The toxicity of **Zn:N-CD** was examined using lung cancer cells (A549), and no noticeable toxicity was observed at concentrations ranging up to 0.5 mg mL^{-1} (Fig. S12, ESI†). Therefore, **Zn:N-CD** is a non-toxic marker with long-lived fluorescence for effectively visualizing latent fingerprints.

Conclusion

The addition of $Zn(OAc)_2$ involves the formation of chemical structures in **Zn:N-CDs**, resulting in improved QY and photostability. An XPS study on the chemical structure variation of the **Zn:N-CD** and **N-CD** samples before and after light exposure revealed that the differences in the chemical structures of the **Zn:N-CD** and **N-CD** samples are related to their photostability. Although further studies are required to clearly understand the role of $Zn(OAc)_2$, the modification of the chemical structures in the CDs by the addition of a catalytic agent can be one of the methods to simultaneously improve the QY and photostability of CDs. As the **Zn:N-CD** developed in this study exhibits strong fluorescence for a long time under light exposure, it can be a good fluorescent material that can be applied in various fields such as in fingerprint detection, cell imaging, therapy, photocatalysis, and energy conversion.

Author contributions

Conceptualization, data curation, funding acquisition, investigation, methodology, project administration, supervision, and writing – review & editing: JC; formal analysis, validation, and visualization: SY and EK; writing – original draft: JC and SY.

Conflicts of interest

There are no conflicts to declare.

Acknowledgements

This work was supported by National Research Foundation of Korea (NRF) grants funded by the Korean government (MSIT) (2020R1C1C1011863 and 2020R1A5A8017671).

Notes and references

1 Y. Choi, Y. Choi, O.-H. Kwon and B.-S. Kim, *Chem.–Asian J.*, 2018, **13**, 586–598.
2 D. Fernandes, M. J. Krysmann and A. Kelarakis, *Chem. Commun.*, 2015, **51**, 4902–4905.
3 R. Das, R. Bandyopadhyay and P. Pramanik, *Mater. Today Chem.*, 2018, **8**, 96–109.
4 F. Yan, Z. Sun, H. Zhang, X. Sun, Y. Jiang and Z. Bai, *Microchim. Acta*, 2019, **186**, 583.
5 H. Ding, X.-H. Li, X.-B. Chen, J.-S. Wei, X.-B. Li and H.-M. Xiong, *J. Appl. Phys.*, 2020, **127**, 231101.
6 M. Liu, *Nanoarchitectonics*, 2020, **1**, 1–12.
7 G. Eda, Y.-Y. Lin, C. Mattevi, H. Yamaguchi, H.-A. Chen, I.-S. Chen, C.-W. Chen and M. Chhowalla, *Adv. Mater.*, 2010, **22**, 505–509.
8 L. Wang, W. Li, L. Yin, Y. Liu, H. Guo, J. Lai, Y. Han, G. Li, M. Li, J. Zhang, R. Vajtai, P. M. Ajayan and M. Wu, *Sci. Adv.*, 2020, **6**, eabb6772.
9 H. Gavilán, E. H. Sánchez, M. E. F. Brollo, L. Asín, K. K. Moerner, C. Frandsen, F. J. Lázaro, C. J. Serna, S. Veintemillas-Verdaguer, M. P. Morales and L. Gutiérrez, *ACS Omega*, 2017, **2**, 7172–7184.
10 Z. Deng, C. Liu, Y. Jin, J. Pu, B. Wang and J. Chen, *Analyst*, 2019, **144**, 4569–4574.
11 H. Sun, L. Wu, N. Gao, J. Ren and X. Qu, *ACS Appl. Mater. Interfaces*, 2013, **5**, 1174–1179.
12 A. Sachdev, I. Matai and P. Gopinath, *RSC Adv.*, 2014, **4**, 20915–20921.
13 X. Li, S. Zhang, S. A. Kulinich, Y. Liu and H. Zeng, *Sci. Rep.*, 2015, **4**, 4976.
14 H. He, Y. Yang, J. Li, X. Lai, X. Chen, L. Wang, W. Zhang, Y. Huang and P. Zhang, *Mater. Sci. Eng., B*, 2021, **264**, 114955.

15 S. Daniel, M. G. Praveena and E. M. Mohammed, *Mater. Sci. Eng., B*, 2021, **269**, 115145.
16 M. Sun, C. Liang, Z. Tian, E. V. Ushakova, D. Li, G. Xing, S. Qu and A. L. Rogach, *J. Phys. Chem. Lett.*, 2019, **10**, 3094–3100.
17 J. Yu, C. Liu, K. Yuan, Z. Lu, Y. Cheng, L. Li, X. Zhang, P. Jin, F. Meng and H. Liu, *Nanomaterials*, 2018, **8**, 233.
18 Y. Li, H. Shu, X. Niu and J. Wang, *J. Phys. Chem. C*, 2015, **119**, 24950–24957.
19 J. Tang, J. Zhang, Y. Zhang, Y. Xiao, Y. Shi, Y. Chen, L. Ding and W. Xu, *Nanoscale Res. Lett.*, 2019, **14**, 241.
20 S. H. Jin, D. H. Kim, G. H. Jun, S. H. Hong and S. Jeon, *ACS Nano*, 2013, **7**, 1239–1245.
21 P. Reineck, A. Francis, A. Orth, D. W. M. Lau, R. D. V. Nixon-Luke, I. D. Rastogi, W. A. W. Razali, N. M. Cordina, L. M. Parker, V. K. A. Sreenivasan, L. J. Brown and B. C. Gibson, *Adv. Opt. Mater.*, 2016, **4**, 1549–1557.
22 B. Ju, Y. Wang, Y.-M. Zhang, T. Zhang, Z. Liu, M. Li and S. Xiao-An Zhang, *ACS Appl. Mater. Interfaces*, 2018, **10**, 13040–13047.
23 N. Javed and D. M. OCarroll, *Part. Part. Syst. Charact.*, 2021, **38**, 2000271.
24 S. Zhu, Q. Meng, L. Wang, J. Zhang, Y. Song, H. Jin, K. Zhang, H. Sun, H. Wang and B. Yang, *Angew. Chem., Int. Ed.*, 2013, **52**, 3953–3957.
25 Y.-Y. Liu, N.-Y. Yu, W.-D. Fang, Q.-G. Tan, R. Ji, L.-Y. Yang, S. Wei, X.-W. Zhang and A.-J. Miao, *Nat. Commun.*, 2021, **12**, 812.
26 J. Zhao, C. Liu, Y. Li, J. Liang, J. Liu, T. Qian, J. Ding and Y.-C. Cao, *Luminescence*, 2017, **32**, 625–630.
27 C. Zhang, L. Du, C. Liu, Y. Li, Z. Yang and Y.-C. Cao, *Results Phys.*, 2016, **6**, 767–771.
28 W. Wang, C. Damm, J. Walter, T. J. Nacken and W. Peukert, *Phys. Chem. Chem. Phys.*, 2016, **18**, 466–475.
29 W. Wang, B. Wang, H. Embrechts, C. Damm, A. Cadranel, V. Strauss, M. Distaso, V. Hinterberger, D. M. Guldi and W. Peukert, *RSC Adv.*, 2017, **7**, 24771–24780.
30 Y. Liu, L. Zhou, Y. Li, R. Deng and H. Zhang, *Nanoscale*, 2017, **9**, 491–496.
31 G. Giesbers, T. D. Krueger, J. D. B. Van Schenck, R. Kim, R. C. Van Court, S. C. Robinson, C. M. Beaudry, C. Fang and O. Ostroverkhova, *J. Phys. Chem. C*, 2021, **125**, 6534–6545.
32 A. Rivaton, A. Tournebize, J. Gaume, P.-O. Bussière, J.-L. Gardette and S. Therias, *Polym. Int.*, 2014, **63**, 1335–1345.
33 I. Ahmad, S. Ahmed, Z. Anwar, M. A. Sheraz and M. Sikorski, *Int. J. Photoenergy*, 2016, **2016**, 8135608.
34 Q. Xu, Y. Liu, R. Su, L. Cai, B. Li, Y. Zhang, L. Zhang, Y. Wang, Y. Wang, N. Li, X. Gong, Z. Gu, Y. Chen, Y. Tan, C. Dong and T. S. Sreeprasad, *Nanoscale*, 2016, **8**, 17919–17927.
35 B. Wang, M. Yang, L. Liu, G. Yan, H. Yan, J. Feng, Z. Li, D. Li, H. Sun and B. Yang, *Biomater. Sci.*, 2019, **7**, 5414–5423.
36 S. K. Tammina, Y. Wan, Y. Li and Y. Yang, *J. Photochem. Photobiol., B*, 2020, **202**, 11734.
37 P. Das, S. Ganguly, M. Bose, S. Mondal, S. Choudhary, S. Gangopadhyay, A. K. Das, S. Banerjee and N. C. Dasa, *Mater. Sci. Eng., C*, 2018, **88**, 115–129.
38 A. Lee, W. Kang and J. Choi, *Nanomaterials*, 2021, **11**, 3046.
39 A. Lee, S. Yun, E. S. Kang, J. W. Kim, J. H. Park and J. Choi, *RSC Adv.*, 2021, **11**, 18776–18782.
40 A. Pal, M. P. Sk and A. Chattopadhyay, *Mater. Adv.*, 2020, **1**, 525–553.
41 X. Miao, D. Qu, D. Yang, B. Nie, Y. Zhao, H. Fan and Z. Sun, *Adv. Mater.*, 2018, **30**, 1704740.
42 M. A. Issa, Z. Z. Abidin, S. Sobri, S. Rashid, M. A. Mahdi, N. A. Ibrahim and M. Y. Pudza, *Nanomaterials*, 2019, **9**, 1500.
43 A. F. Shaikh, M. S. Tamboli, R. H. Patil, A. Bhan, J. D. Ambekar and B. B. Kale, *J. Nanosci. Nanotechnol.*, 2019, **19**, 2339–2345.
44 A. B. Siddique, A. K. Pramanick, S. Chatterjee and M. Ray, *Sci. Rep.*, 2018, **8**, 9770.
45 P. M. Gharat, J. M. Chethodil, A. P. Srivastava, Praseetha P. K., H. Pal and S. Dutta Choudhury, *Photochem. Photobiol. Sci.*, 2019, **18**, 110–119.
46 M. K. Barman and A. Patra, *J. Photochem. Photobiol., C*, 2018, **37**, 1–22.
47 C. M. Carbonaro, R. Corpino, M. Salis, F. Mocci, W. V. Thakkar, C. Olla and P. C. Ricci, *C*, 2019, **5**, 60.
48 M. L. Liu, B. B. Chen, C. M. Li and C. Z. Huang, *Green Chem.*, 2019, **21**, 449–471.
49 X. Kou, S. Jiang, S.-J. Park and L.-Y. Meng, *Dalton Trans.*, 2020, **49**, 6915–6938.
50 H. Zheng, P. Zheng, L. Zheng, Y. Jiang, Z. Wu, F. Wu, L. Shao, Y. Liu and Y. Zhang, *J. Phys. Chem. C*, 2018, **122**, 29613–29619.
51 M. Zulfajri, G. Gedda, C.-J. Chang, Y.-P. Chang and G. G. Huang, *ACS Omega*, 2019, **4**, 15382–15392.
52 F. Rafiee, N. Tajfar and M. Mohammadnejad, *Int. J. Biol. Macromol.*, 2021, **189**, 477–482.
53 S. Dinant, N. Wolff, F. De Marco, F. Vilaine, L. Gissot, E. Aubry, C. Sandt, C. Bellini and R. Le Hir, *J. Exp. Bot.*, 2019, **70**, 871–884.
54 J. Cheng, C.-F. Wang, Y. Zhang, S. Yang and S. Chen, *RSC Adv.*, 2016, **6**, 37189–37194.
55 S. Hu, A. Trinchi, P. Atkin and I. Cole, *Angew. Chem., Int. Ed.*, 2015, **54**, 2970–2974.
56 Y. Nie, X. Zhi, H. Du and J. Yang, *Molecules*, 2018, **23**, 760.
57 Y. Qin, D. Zhou and M. Li, *Lett. Org. Chem.*, 2012, **9**, 267–272.
58 I. Milenkovic, M. Algarra, C. Alcoholado, M. Cifuentes, J. M. Lázaro-Martínez, E. Rodríguez-Castellón, D. Mutavdžić, K. Radotić and T. J. Bandosz, *Carbon*, 2019, **144**, 791–797.
59 C. Wang, J. Zhou, L. Lulu and Q. Song, *Part. Part. Syst. Charact.*, 2018, **35**, 1700387.